OFF-AXIS DRAG OF DENDRITE FRAGMENTS AT LOW REYNOLDS NUMBER

NASA Contract NCC3-272

FINAL REPORT: September 1, 1992 - August 31, 1994

by

P. D. Weidman

Department of Mechanical Engineering
Campus Box 427
University of Colorado
Boulder, CO 80309

1. INTRODUCTION

The aim of the present investigation is to characterize the motion of dendrite fragments falling under the influence of gravity in a uniform liquid medium at low Reynolds number. In an earlier study, Zakhem, Weidman and de Groh (1992) reported on the settling speed of model equiaxed dendrite grains released along their axis of symmetry. In this follow-up study uniaxial model dendrite grains were released off-axis to observe and document their motion at different orientations. It was hypothesized that the dendrite models might rotate when released off-axis in which case an attempt would be made to document the ensuing unsteady motion. This latter event turned out to be in fact true: at the small but finite Reynolds numbers that existed, each uniaxial dendrite slowly rotated towards its equilibrium orientation while falling under the influence of gravity.

In addition to completing the original goal, we have made use of a beads-on-a shell Stokes flow code to numerically determine the drag coefficient for capsules, *i.e.*, uniaxial dendrites without arms. The drag on horizontally and vertically falling capsules are reported and compared with measurements.

2. TEST PROCEDURE

The experiments were conducted in the large tank Stokes flow tank shown in Figure 1. The apparatus is of square cross section measuring 61 cm X 61 cm X 91 cm and contains 90 gallons of Dow Corning silicone oil as the test fluid. Details of the test measurement procedure are given below.

Initial observations of the motion of uniaxial dendrites released off-axis showed that the motion was inherently unsteady as a result of the dendrite seeking its minimum drag orientation. Hence we abandoned the laser system system sketched in Figure 1, which is suitable only for steady flow, and replaced it with a photographic data acquisition system. A Nikon camera placed approximately twelve feet horizontally away from the center section of the test facility was devised to fire electronically at arbitrary periods in the range 2-150 sec/frame. Position measurements were taken from a ruled sheet taped to the back wall of the facility. Parallax effects were removed by photographing a second grid placed in the mid-plane of the apparatus filled with the test fluid. Figures 2a,b exhibit the raw data for the mid-plane calibration while Figures 2c,d give the raw data for calibration of the back wall grid. This data is then used to arrive at the parallax correction equations

$$Y_{mp} = 2.54\ [1.11589\ (0.5\ Y_{bw}) + 0.04766] \tag{2.1}$$

$$X_{mp} = 2.54\ [1.07755\ (0.5\ X_{bw}) - 0.00634] \tag{2.2}$$

which gives the mid-plane coordinates X_{mp} and Y_{mp} in terms of the fixed grid back wall coordinates X_{bw} and Y_{bw} with a conversion factor to convert to centimeters.

Another important modification of the test facility was the design and construction of a spring actuated release mechanism that could initially orient the dendrites at arbitrary angles θ relative to the vertical as defined in Figure 4. Dendrites with appendages, such as models U2 and U3 shown in Figure 4, were always released with the stalk and two or more arms in the mid-plane and the remaining arms perpendicular to the mid-plane. The expectation was that the dendrites would slowly rotate in θ towards its final equilibrium position. It turns out, however, that the dendrites also rotated about their central axis. This defines a second angle ϕ as sketched in Figure 4.

The density and viscosity of the silicone oil test fluid were accurrately measured as a function of temperature following the procedure outlined in Lasso and Weidman (1986). The results are

$$\rho = 1.0123 - 0.0015176\ T \qquad (g/cm^3, \text{ with T in } ^\circ C) \qquad (2.3)$$

$$\nu = 7895.15 - 199.19\ T + 2.8899\ T^2 \qquad (mm^2/sec, \text{ with T in } ^\circ C) \qquad (2.4)$$

Uniaxial dendrites like those sketched in Figure 4 were tested. The labeling sequence for the models is U0, U1, U2 and U3 where the number denotes the number of planes of four arm appendages. Note that the U1 dendrite is not shown in Figure 4. In adition we distinguish between small and big, light and heavy geometrically similar models with letters S and B, L and H, respectively. The suffixes A and B attached to U0 through U3 pertain to different primary rod aspect ratios ℓ/a. The dendrite U0 without appendages will be referred to as a capsule. Although twenty uniaxial dendrite models were constructed for the along-axis tests reported in Zakhem, *et al.* (1992), some were broken in the interim and only sixteen survived in tact. The physical dimensions of each uniaxial model used in the present experiments are given in Table I.

3. RESULTS

The measurements presented here will be divided into to parts: capsules and dendrites with arms. In the preceeding study by Zakhem, *et al.* (1992) all dendrites were released along a central axis and in the case of uniaxial dendrites the arms were facing down. When the dendrites were released with out significant disturbance, they were observed to fall without significant tilting off the central axis of the tank. Those measurements thus constitute steady flow drag results for the orientation $\theta = \pi$ and it appeared that this was the equilibrium position of dendrites with arms. In the present investigation two other steady flow orientations are observed. For a capsule carefully released at $\theta = \pi/2$ the capsule remained horizontal and the flow was basically steady. However, this orientation is one of neutral equilibrium since the drag is larger for horizontally falling capsules than for vertically falling capsules. Releasing the capsule slightly off horizontal causes them to rotate gently towards its minimum drag position at $\theta = 0$ or π. These results will be discussed in §3.1. The second steady flow orientation is $\theta = 0$ for dendrites with arms; all U1, U2 and U3 dendrites released horizontally at $\theta = \pi/2$ immediately rotated towards their equilibrium positions at $\theta = 0$ with dendrite arms up. Results for the motion of dendrites with arms will be given in §3.2.

3.1 Capsules

Capsules released horizontally and vertically moved steadily down the axis of the tank with out appreciable rotation. The *ad hoc* correction procedure to back out blockage and inertial effects developed by Lasso and Weidman (1986) and used successfully by Zakhem, *et al.* (1992) and Roger and Weidman (1998) cannot be used for horizontally-oriented dendrites. This is because the dendrite is no longer axisymmetric with respect to the tank centerline and the results of Wakiya (1957) cannot be used to obtain the wall correction factor K_w. However, a reasonable estimate of the dimensionless horizontal capsule drag $D/\mu RU$, where $R = a/2$ and $U = U_s$ is the Stokes settling speed, can be obtained using the vertical capsule drag results of Zakhem, *et al.* (1992). Assuming that the Sutterby correction factor K for both horizontally and vertically falling capsules as a function of ℓ/a are of the same order, ranging from 3-6% of the total drag for all capsules except U0ABH. Since $U_s = KU_m$ where U_m is the *in situ* measured descent velocity, the ratios $(U_s)_v/(U_s)_h$ and $(U_m)_v/(U_m)_h$ will be almost equal. Then the horizontal drag coefficient will be given by

$$\left[\frac{D}{\mu RU}\right]_h = \frac{(U_m)_v}{(U_m)_h}\left[\frac{D}{\mu RU}\right]_v \tag{3.1}$$

where $(D/\mu RU)_v$ is taken from Zakhem, *et al.* (1992). We have measured both horizontally and vertically falling descent rates and the calculations are summarized in Table II.

Theoretical values of the dimensionless drag ratios for vertically and horizontally falling capsules have been calculated as a function of ℓ/a using the beads-on-a-shell numerical method used extensively by Roger and collaborators (Roger and Hussey 1982, Ui, *et al.* 1984). Basically, the object is covered by an array of contiguous Stokeslets in the form of small diameter beads and the hydrodynamic interaction between all pairs of beads are calculated. If d is the bead diameter, then the drag is obtained by extrapolation to zero d/a. The method is concisely reviewed by Roger and Weidman (1998).

An example of the coverage of a capsule by small Stokeslet beads is given in Figure 5 for $\ell/a = 4.30$. A coarse covering at $d/a = 0.08$ and a fine covering at $d/a = 0.04$ are exhibited. A test of the extrapolation to zero bead size is shown in Figure 6(a) for drag on a sphere; here NR is the number of rings of beads surrounding the sphere. The extrapolation from $d/a = 0.018$ to zero bead size indeed accurately gives the sphere drag $6\pi\mu UR$ where $R = a/2$ is the radius of the sphere. An example of a calculation for a vertically falling capsule is given in Figure 6(b). Here it is evident that one must go to much smaller values of d/a in order to obtain a good extrapolation to zero bead size. Extensive calculations gives the summary data for horizontally and vertically falling spheres shown in Figure 7(a). The difference in drag between horizontally and vertically falling spheres increases montonically with the capsule aspect ratio ℓ/a and the two drags merge at $\ell/a = 1$ since that point corresponds to a sphere in both cases. A good fit to the numerically computed data points over the range $1 \leq \ell/a \leq 8$ is given by

$$\left[\frac{D}{\mu RU}\right]_v = 8.70126 + 10.9262\left[\frac{\ell}{a}\right] - 0.900089\left[\frac{\ell}{a}\right]^2 + 0.0390386\left[\frac{\ell}{a}\right]^3 \tag{3.2}$$

$$\left[\frac{D}{\mu RU}\right]_h = 8.53559 + 10.9518\left[\frac{\ell}{a}\right] - 0.760142\left[\frac{\ell}{a}\right]^2 + 0.0407061\left[\frac{\ell}{a}\right]^3. \tag{3.3}$$

The experimental results listed in Table II are compared with the theoretically determined drag curves in Figure 7(b). The values for vertically falling capsules are the original U0ASL, U0BSL and U0BSL results of Zakhem, *et al.* chosen because they have the least inertial and wall corrections. The values for horizontally falling capsules are an average of the present measurements of U0ASL and U0ASH at $\ell/a = 3.50$, of U0ABL and U0ABH at $\ell/a = 3.71$, and include the single result for U0BBH at $\ell/a = 8.00$. The measurements are in good agreement with the theoretical calculations considering that the blockage and inertial effects on the horizontally falling capsules have only been estimated.

It should be borne in mind that the horizontally falling capsules are only neutrally stable. Capsules released slightly off horizontal were observed to rotate away towards vertical. The time variation of this rotation for capsules U0ASL and U0BSH are shown in Figure 8. Given in the insets are the *in situ* Reynolds numbers

$$(Re)_{a_r} = \frac{\rho a_r U_m}{\mu} \tag{3.4}$$

in which a_r is the radius of a sphere formed by the volume of the dendrite model. Note in

Figure 8(a) that the U0ASL dendrite released at approximately $\theta_0 = 81°$ rotates only 2.5° during its descent, but it is definitely rotating towards its minimum drag orientation at $\theta = 0°$. The U0BSH dendrite in Figure 8(b) released much nearer neutral stability at $\theta_0 = 85°$ rotates a full 10° during its descent towards the vertical equilibrium position. The faster rotation of the latter dendrite is due to its increased inertia and increased aspect ratio which provides a higher rotational torque once off neutral equilibrium: the Reynolds number of the U0BSH dendrite is about five times and the aspect ratio is about double that of the U0ASL dendrite.

3.2 Dendrites

All dendrites rotated away from their initial position when released horizontally, however none reached the vertical equilibrium orientation in the limited height of the test facility. Consequently, ach dendrite was released at different initial angles θ_0 in an attempt to observe the entire rotation process from θ_0 near $\pi/2$ to the vertical equilibrium position with arms upward. Separate rotation curves were matched in a systematic manner to produce a composite plot of θ *versus* time. The results for U1 dendrites are given in Figure 9, for U2 dendrites in Figure 10, and for U3 dendrites in Figure 11. Here different symbols denote different experimental runs. While most curves matched well to form the composit curve, some did not. Close scrutiny of the photographs revealed that the reason for the mismatch of some curves was due to the fact that some dendrites rotated about their central axis, corresponding to the angle ϕ sketched in Figure 4. In several instances the dendrites rotated a full 45° to a position of new reflective symmetry about the mid-plane. This evidently represents a least-drag configuration compared to the release orientation with two arms in the mid-plane and two arms perpendicular to the mid-plane, also a position of reflective symmetry.

The basic feature to note is that the dendrites exhibit their maximum rotation rate near $\theta = \pi/2$, almost without exception. To see this, one must look at the local slopes defined by the plotted data points and not at the polynomial curve fitting the composite data set. That the maximum rotation rate is at $\pi/2$ is reasonable since the dendrite arms are fartherest from the dendrite centroid and hence cause the greatest torque at finite Reynolds numbers. Of course at zero Reynolds number the dendrites would not rotate because of the absence of inertial effects. A characterization of the rotational motion can be obtained by plotting the rotation rate of each dendrite at $\theta = \pi/2$ against $(Re)_{a_r}$ according to equation (3.4). Although these data listed in Table III did show some systematic behavior, the results did not collapse well. Since a_r does not measure the fractal-like nature of the dendrites, it was thought that a Reynolds number based on the shape length scale $L_s = 3V/A$, where V is the dendrite volume and A is its surface area, might provide a better correlation. Thus in Figure 12 we have plotted $\theta(\pi/2)$ *versus* $(Re)_{L_s}$, where

$$(Re)_{L_s} = \frac{\rho L_s U_m}{\mu}. \tag{3.5}$$

The average aspect ratio of the stalks is $\ell/a = 4.10$; both U1 and U2 dendrites have $\ell/a = 3.80$ while the U3 dendrites have $\ell/a = 4.40$. The limited number of data points in this log-linear plot suggest a rather sharp transition from slowly rotating dendrites at $(Re)_{L_s} < 0.005$ to more rapidly rotating dendrites at $(Re)_{L_s} > 0.005$. The different behaviors between U2 and U3 dendrites at large $(Re)_{L_s}$ is evidently due primarily to the different distribution of the dendrite arms about the centroid which causes different torques. There may also be a small influence of the different aspect ratios of the two dendrites.

4 SUMMARY AND CONCLUSION

The primary findings of this investigation are:

1) Capsules have two equilibria; horizontally falling capsules are neutrally stable and vertically falling capsules are absolutely stable.

2) Dendrites have two equilibira; vertically falling dendrites with arms downward are neutrally stable and vertically falling dendrites with arms upward are absolutely stable.

3) Drag *versus* aspect ratio curves for horizontally and vertically falling capsules have been computed by the BoS method. These results are in reasonable agreement with experimental measurements at the three aspect ratios where data are available.

4) Dendrites released horizontally rotate towards equilibrium with maximum rotation rates observed near $\theta = \pi/2$. A plot of these rates *versus* the Reynolds number based on the shape length scale L_s reveals a sharp transition between slow and fast dendrite rotation rates near $(Re)_{L_s} = 0.005$.

5) Dendrites released with stalk and two opposing sets of arms coincident with a vertical plane that includes gravity, rotate in ϕ about the stalk axis while rotating in θ about their centroids. The equilibrium position in ϕ is the one for which all dendrite arms are oriented at the angle $\phi = \pi/4$ with respect to the mid-plane.

The results found in this study can be used to estimate the orientation of dendrite fragments when they freeze in a solidifying melt. The descent rates of the dendrites do not vary much with orientation, and so the earlier results of Zakhem, *et al.* (1992) can be used to estimate the settling speeds of arbitrarily oriented dendrites. The rotation rates of the dendrites, however, are a strong function of Reynolds number, even at near Stokes flow conditions.

References

Lasso, I. and Weidman, P. D. *Phys. Fluids*, 29, 3921 (1986).

Roger, R. P. and Hussey, R. G. *Phys. Fluids*, 25, 915 (1982).

Roger, R. P. and Weidman, P. D. *Euro. J. Mech. B/Fluids*, to appear 1998.

Ui, T. J., Hussey, R. G. and Roger, R. P. *Phys. Fouids*, 27, 787 (1984).

Wakiya, S. *J. Phys. Japan*, 12, 1130 (1957).

Zakhem, R., Weidman, P. D. and de Groh, H. C. *Metall. Trans. A*, 23, 2169 (1992).

Model	l	a	a'	b	b'	b''	c	c'	c''
U0A S	2.223	0.635	—	—	—	—	—	—	—
U0A B	4.709	1.270	—	—	—	—	—	—	—
U0B S	2.540	0.318	—	—	—	—	—	—	—
U0B B	5.080	0.635	—	—	—	—	—	—	—
U1 S	2.413	0.635	0.114	1.905	—	—	0.762	—	—
U1 B	4.826	1.270	0.241	3.810	—	—	1.524	—	—
U2 S	2.413	0.635	0.114	1.905	1.466	—	0.762	1.143	—
U2 B	4.826	1.270	0.241	3.810	2.934	—	1.524	2.286	—
U3 S	2.794	0.635	0.114	2.032	1.905	1.466	0.762	1.143	1.524
U3 B	5.588	1.270	0.241	4.064	3.810	2.934	1.524	2.286	3.048

Table I. Physical dimensions of the 10 groups of model dendrites.
(All dimensions are in units of centimeters.)

Model	$(U_m)_h$	$(U_m)_v$	$(U_m)_v/(U_m)_h$	$(D/\mu RU)_v$	$(D/\mu RU)_h$
U0ASL	0.1002	0.1187	1.185	36.89	43.71
U0ASH	0.6110	0.7209	1.179	34.26	40.41
U0ABS	0.3859	0.4509	1.168	36.36	42.47
U0ABH	2.321	2.756	1.187	35.10	41.66
U0BSL	-	-	-	52.85	-
U0BSH	-	-	-	53.37	-
U0BBL	-	-	-	55.26	-
U0BBH	0.8S35	1.1220	1.3624	53.26	72.55

Table II. Measured capsule descent rates and calculated dimensionless drags.
(All velocities in units of cm/sec.)

Model	T	U_m	a_r	$(Re)_{a_r}$	ℓ/a	$\theta(\pi/2)$	a_r/L_s	$(Re)_{L_s}$
U0ASL	23.6	0.1061	0.534	0.001252	8.00	-	-	-
U0BSH	24.5	0.0324	0.358	0.000261	3.50	-	-	-
U1SL	25.8	0.0992	0.575	0.001313	3.80	0.125	1.569	0.000834
U1BL	25.3	0.3293	1.155	0.008674	3.80	0.333	1.569	0.00553
U2SH	24.0	0.669	0.590	0.00879	3.80	0.742	1.734	0.00506
U2BL	23.9	0.339	1.188	0.00894	3.80	0.133	1.734	0.00515
U2BH	24.5	2.391	1.188	0.0638	3.80	1.368	1.734	0.0368
U3SH	24.0	0.721	0.638	0.01023	4.40	0.642	1.995	0.00513
U3BL	24.3	0.359	1.288	0.01036	4.40	0.173	1.995	0.00519
U3BH	24.2	2.642	1.288	0.0760	4.40	1.242	1.995	0.03811

Table III. Measured capsule descent rates and calculated dimensionless drags. (Temperatures in °C, velocities in cm/sec, and lengths in centimeters.)

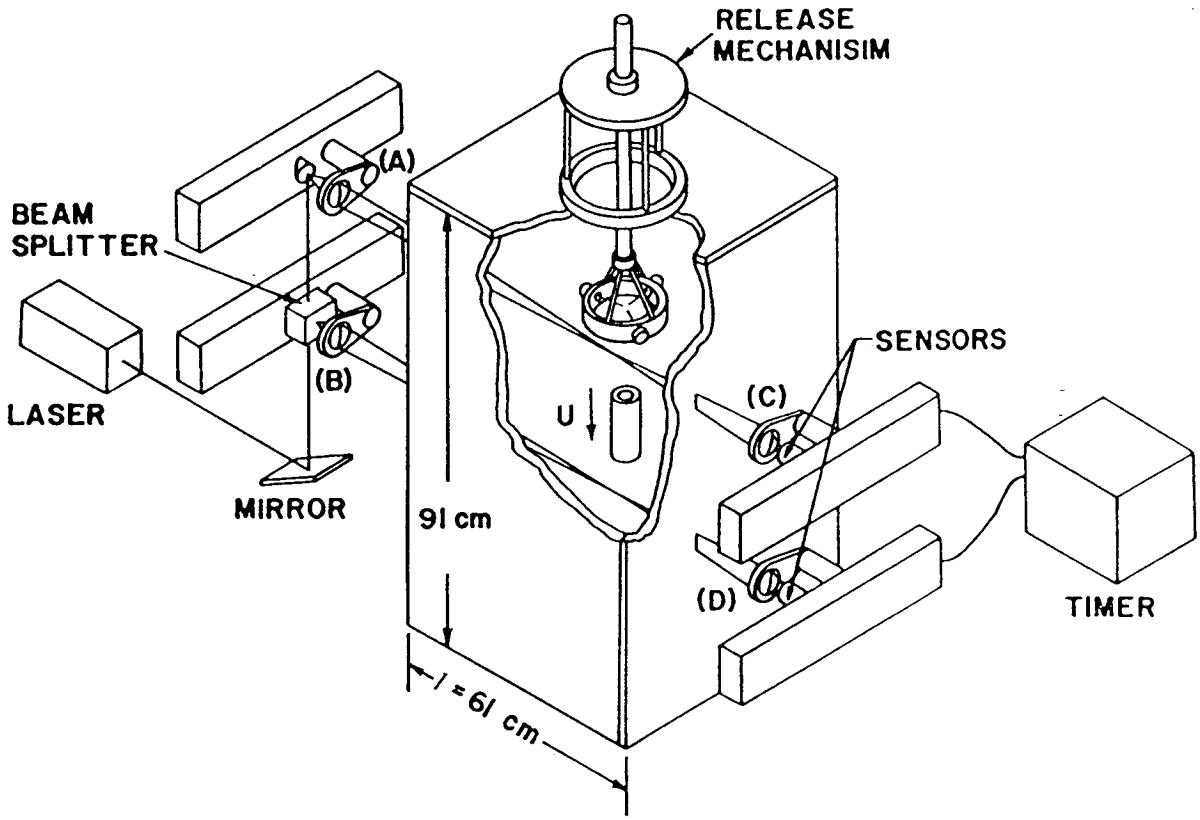

Figure 1. Experimental facility.

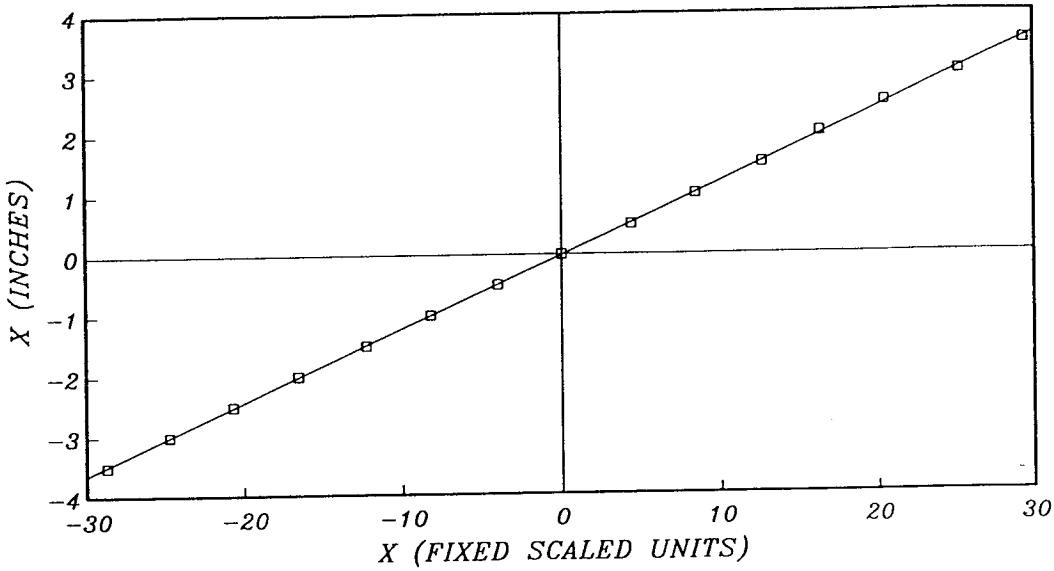

Figure 2(a). Mid-plane horizontal grid calibration curve.

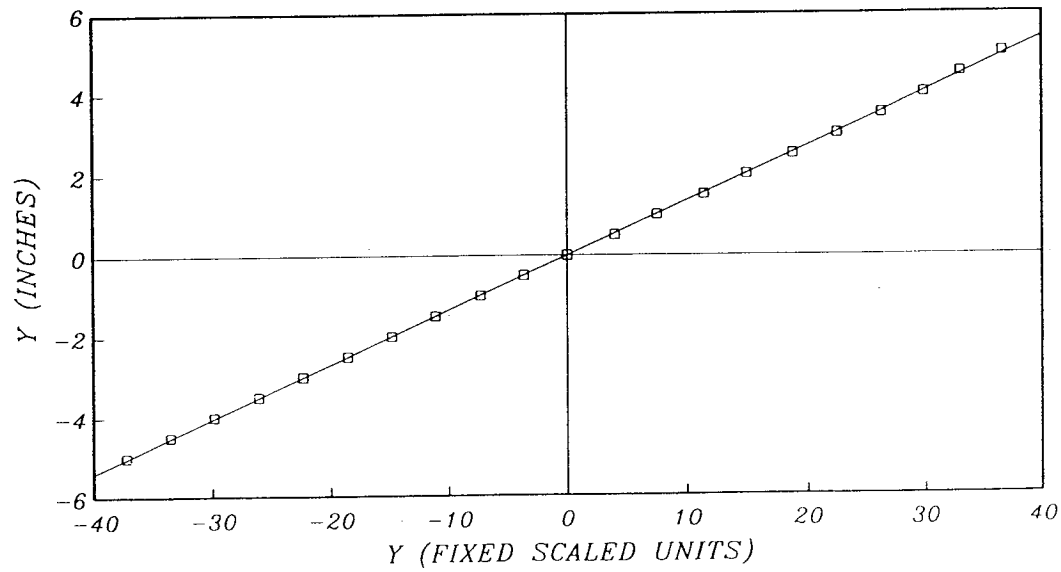

Figure 2(b). Mid-plane vertical grid calibration curve.

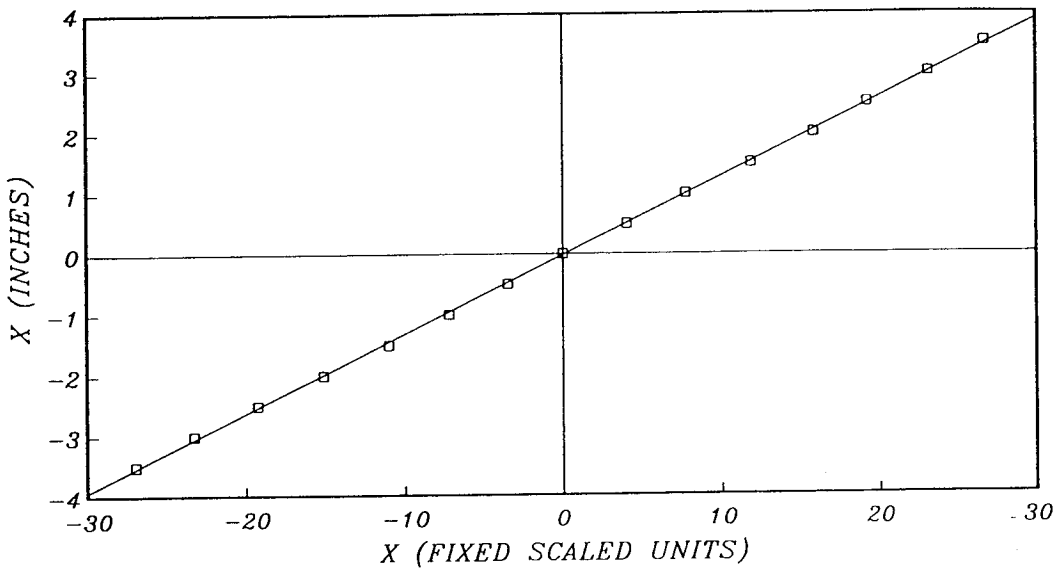

Figure 2(c). Back wall horizontal grid calibration curve.

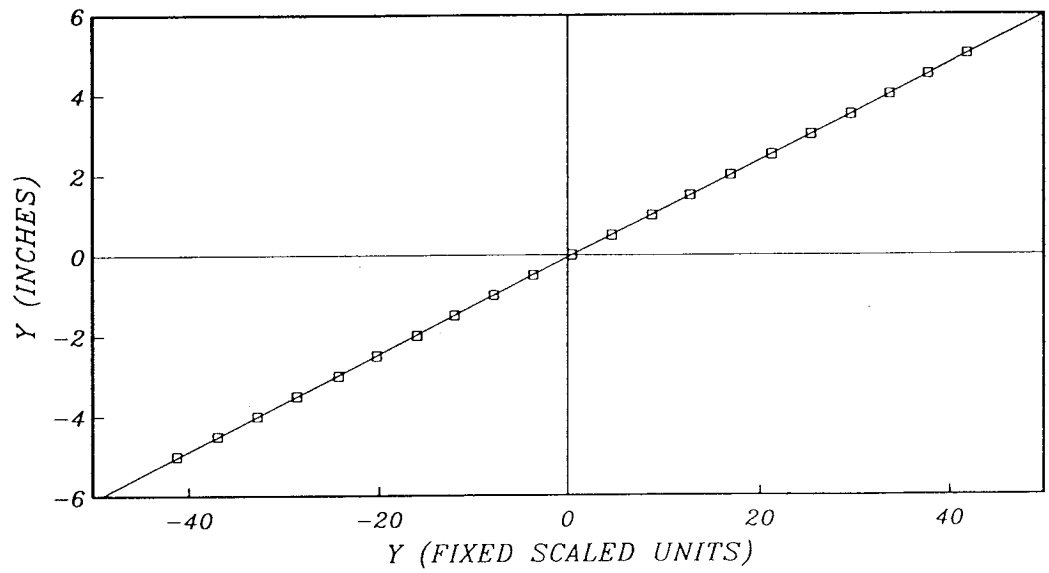

Figure 2(d). Back wall vertical grid calibration curve.

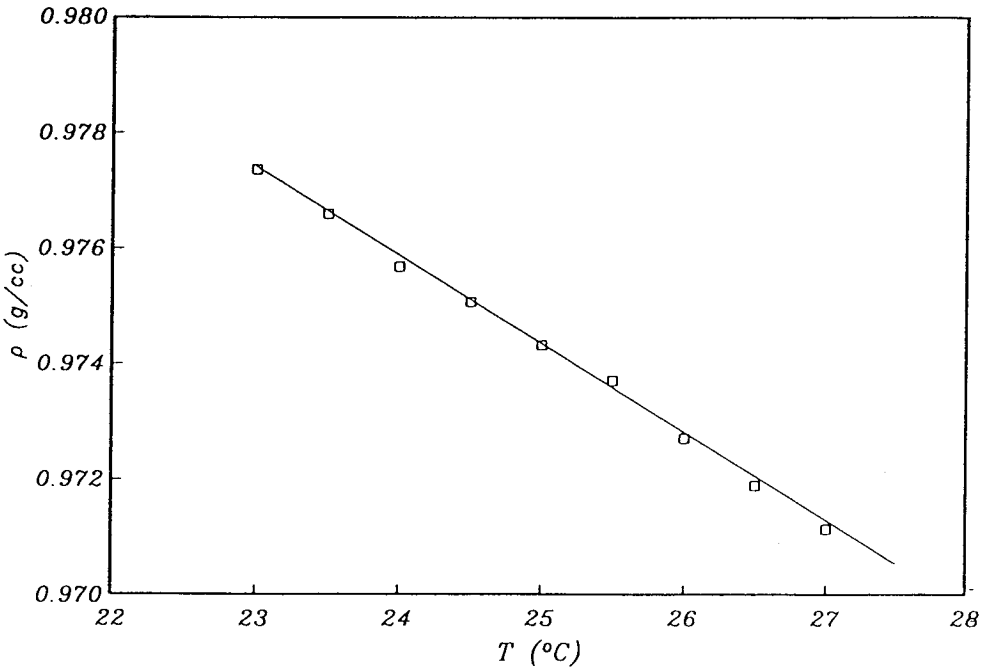

Figure 3(a). Temperature variation of density for the silicone oil test fluid.

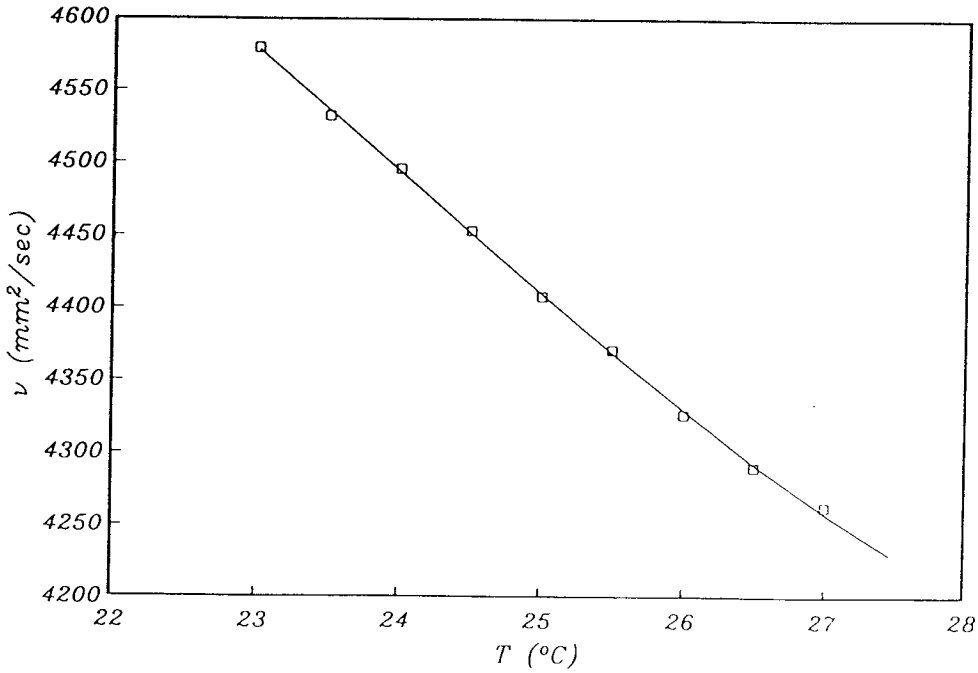

Figure 3(b). Temperature variation of viscosity for the silicone oil test fluid.

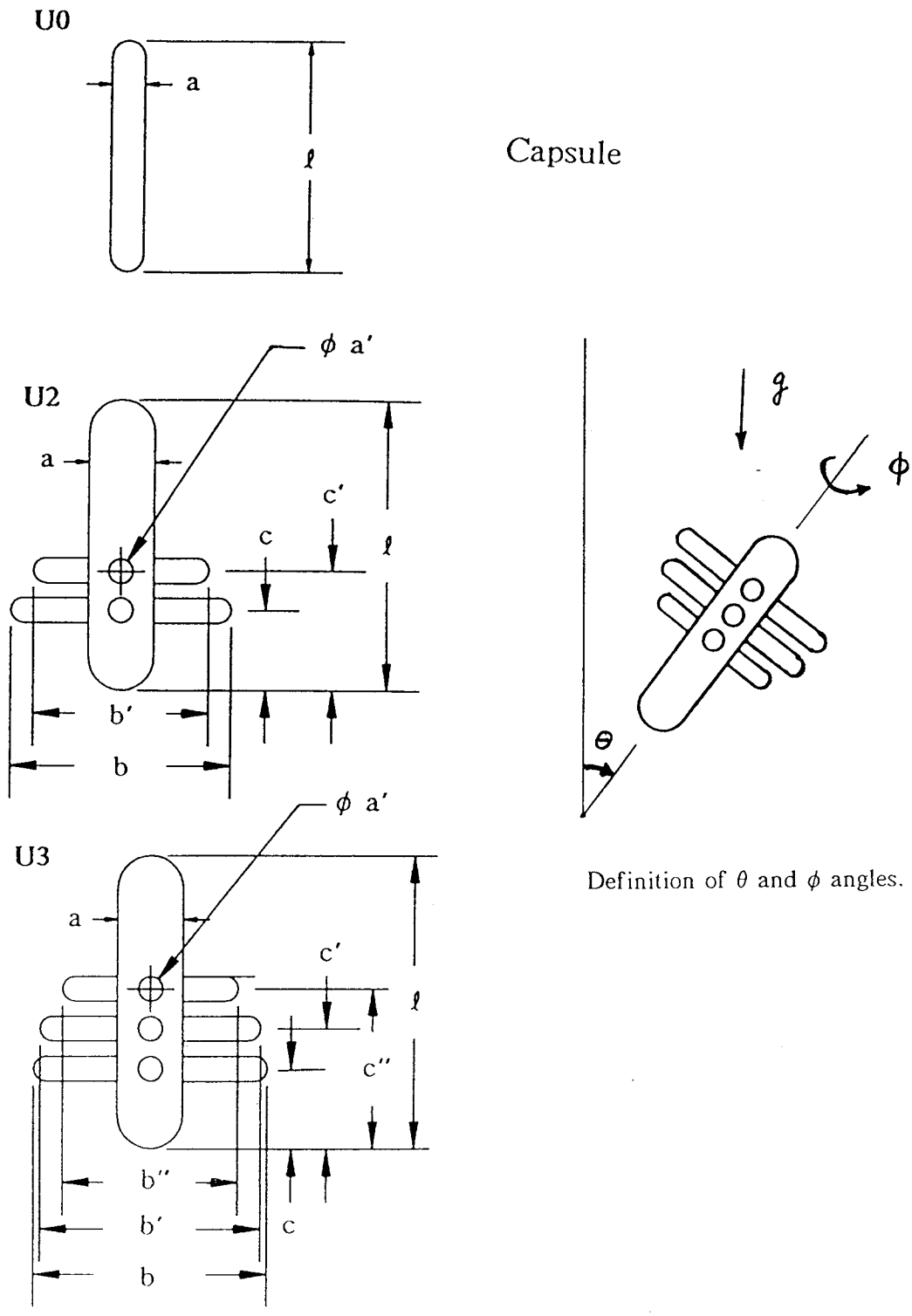

Definition of θ and ϕ angles.

Figure 4. Geometry of the model uniaxial dendrites.

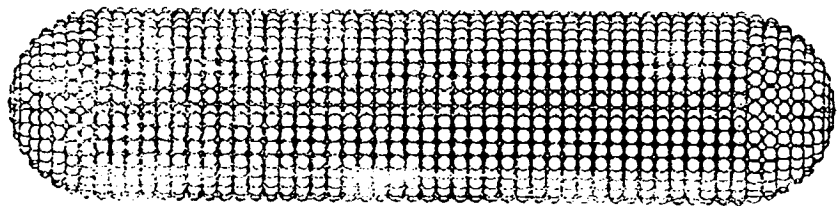

d/a = 0.08

ℓ/a = 4.30

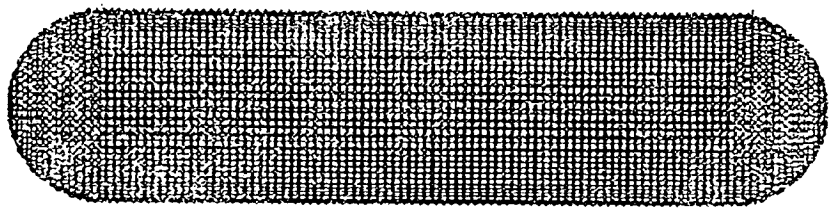

d/a = 0.04

Figure 5. Model capsule constructed for two different bead sizes.

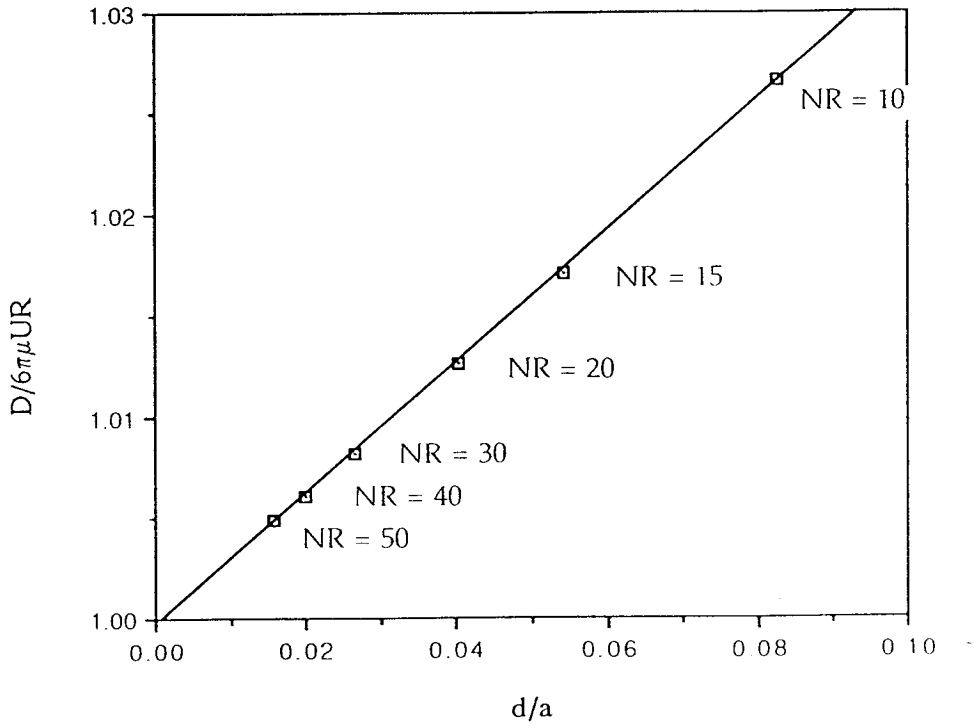

Figure 6(a). Extrapolation to zero d/2a for BoS Stokes drag of a sphere.

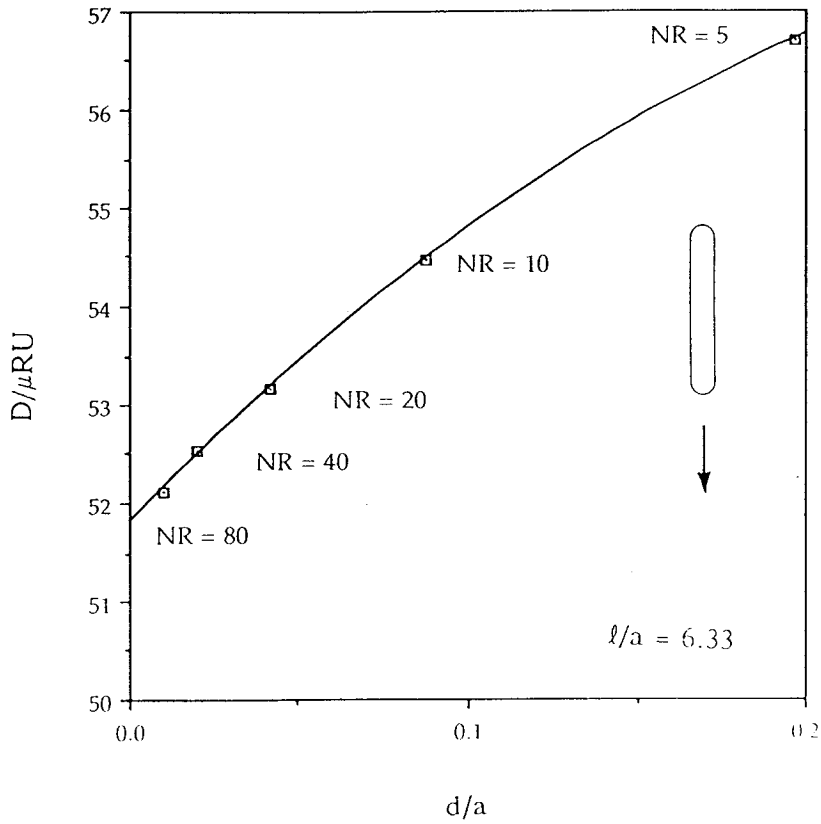

Figure 6(b). Extrapolation to zero d/2a for BoS Stokes drag of a capsule.

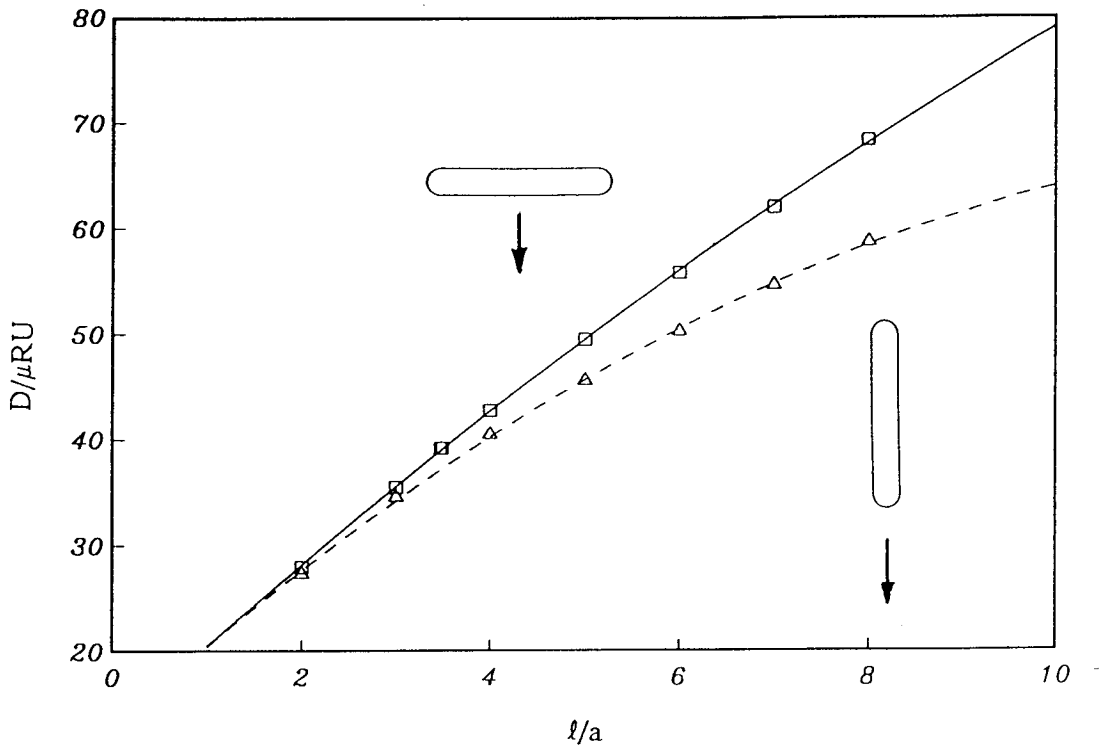

Figure 7(a). BoS computed drag curves for horizontally and vertically falling capsules.

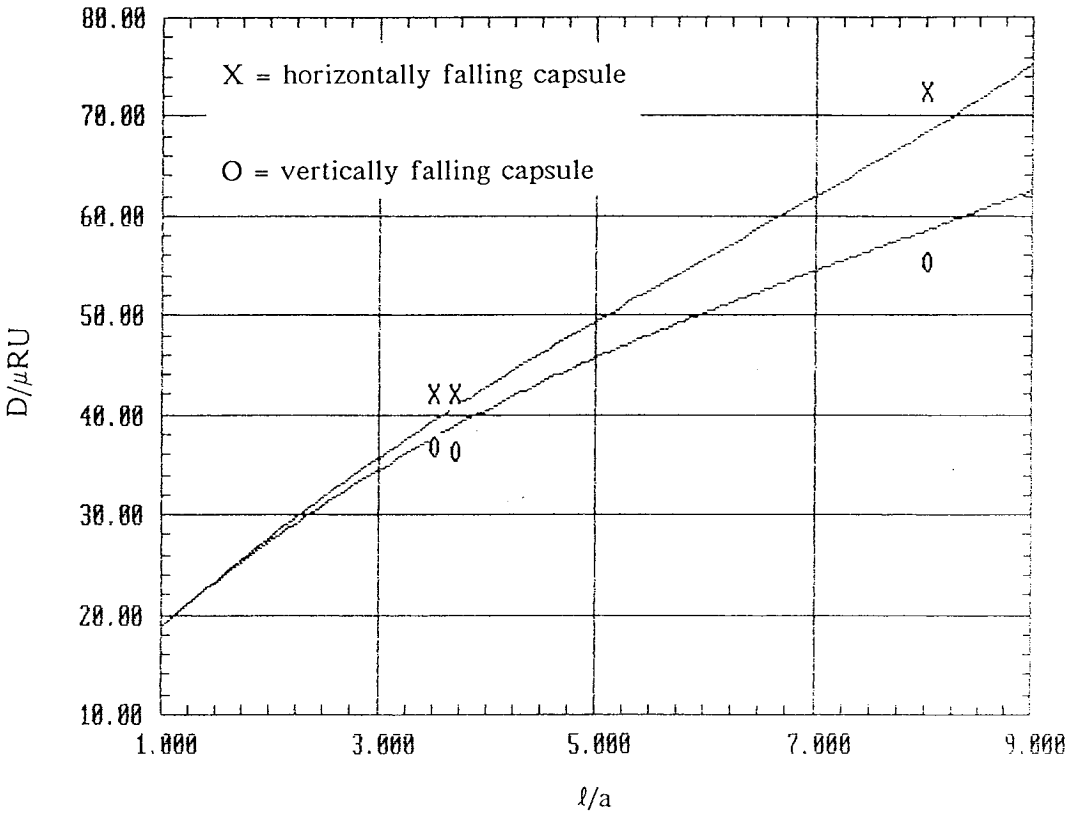

Figure 7(b). Comparison of experimental measurements with BoS computations.

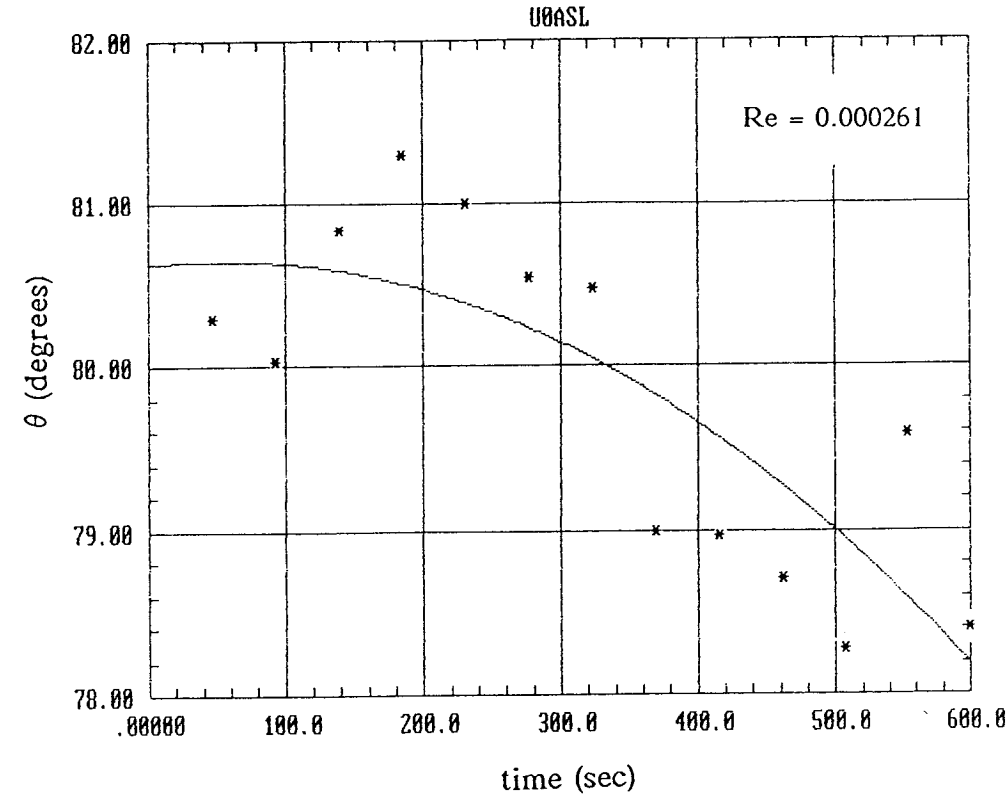

Figure 8(a). Time variation of θ for U0ASL dendrite with ℓ/a = 3.50.

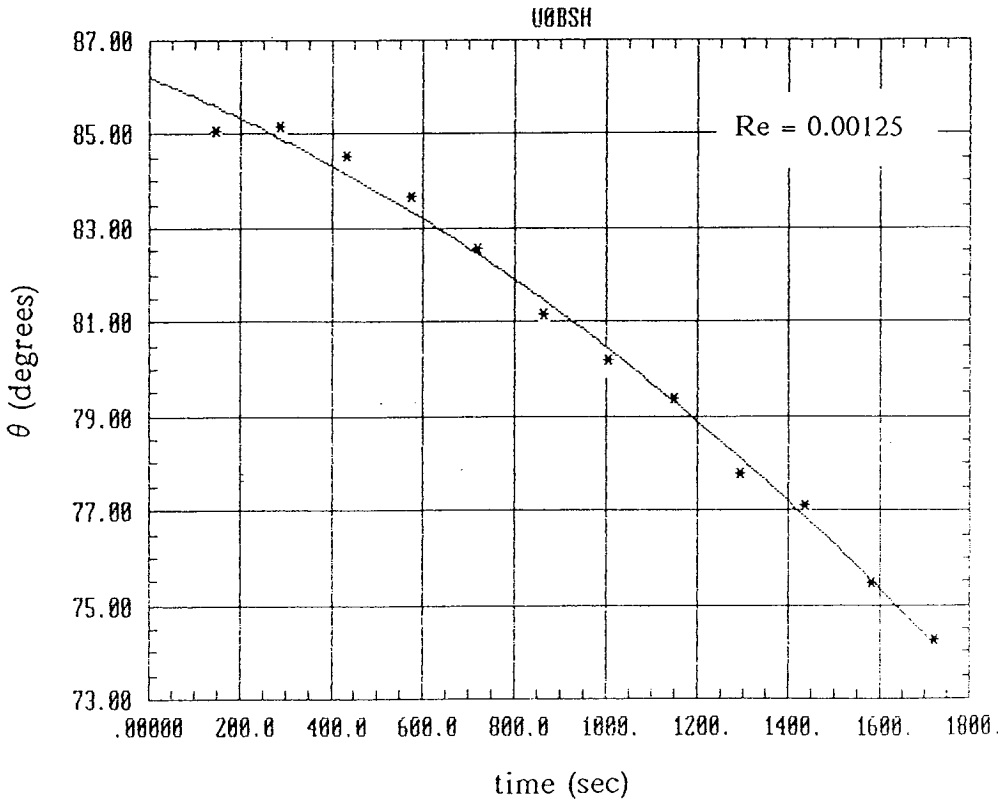

Figure 8(b). Time variation of θ for U0BSH dendrite with ℓ/a = 8.00.

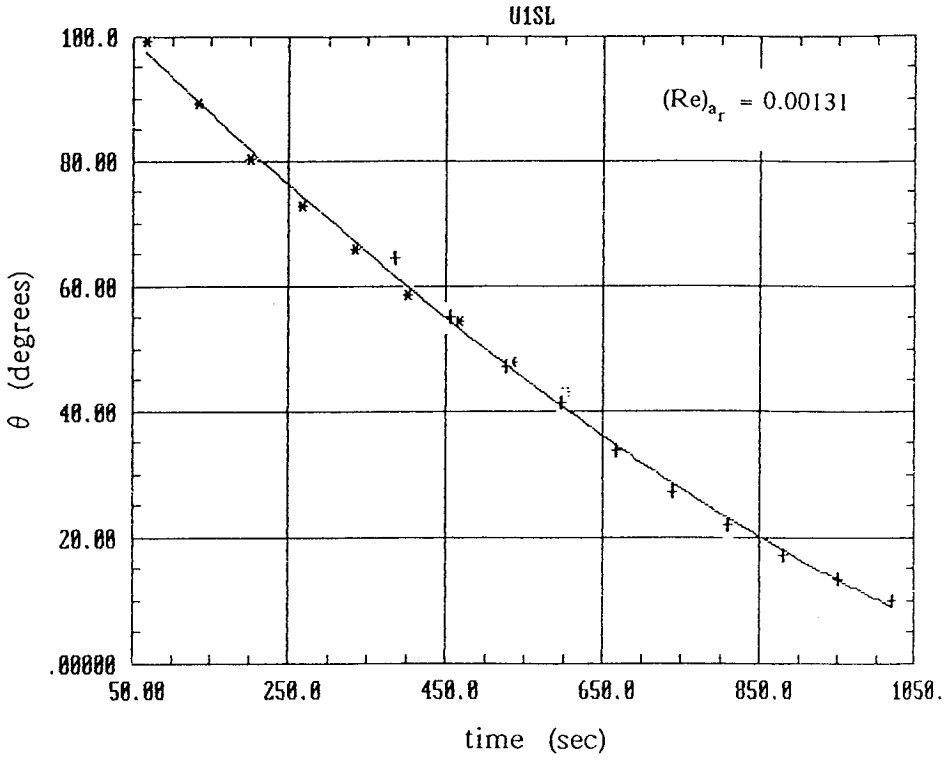

Figure 9(a). Time variation of θ for U1SL dendrite with ℓ/a = 3.80.

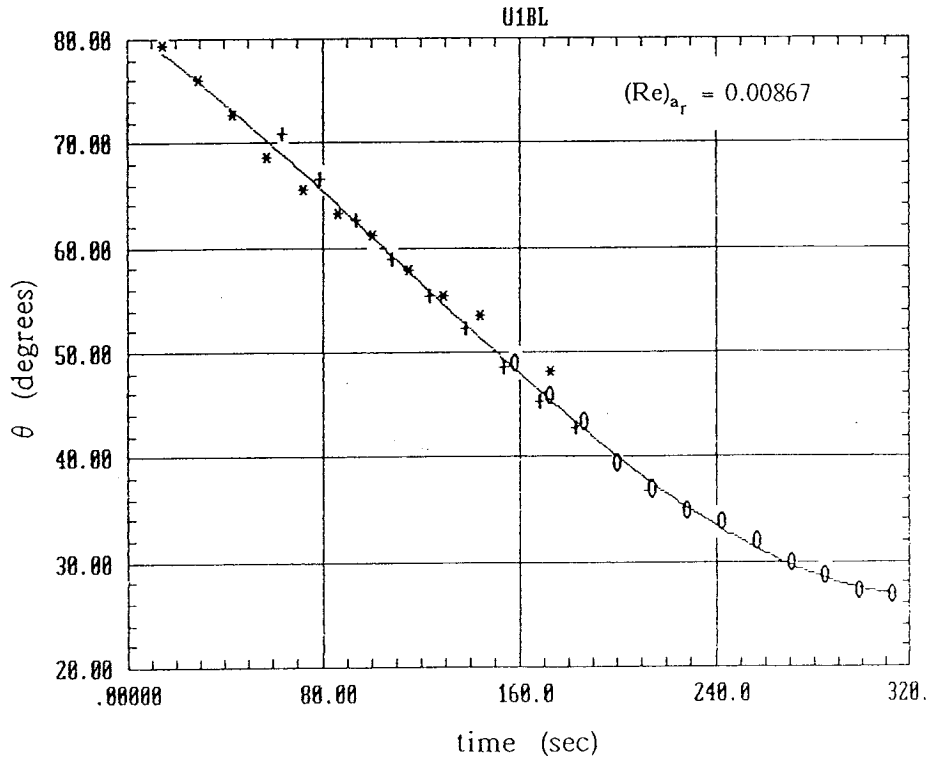

Figure 9(b). Time variation of θ for U1BL dendrite with ℓ/a = 3.80.

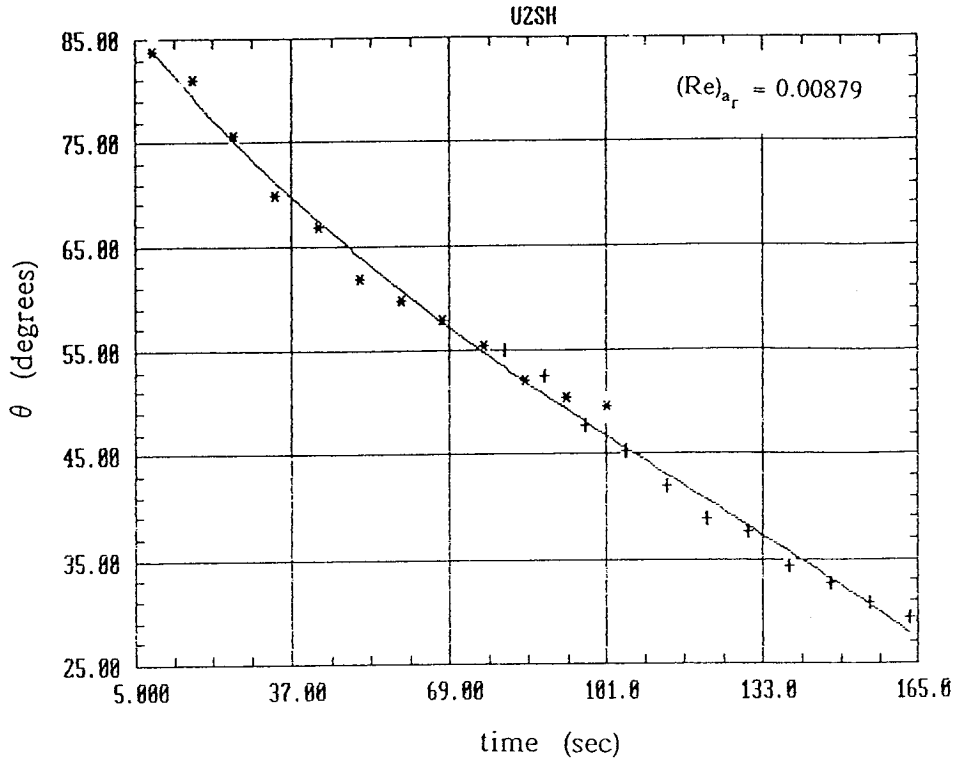

Figure 10(a). Time variation of θ for U2SH dendrite with ℓ/a = 3.80.

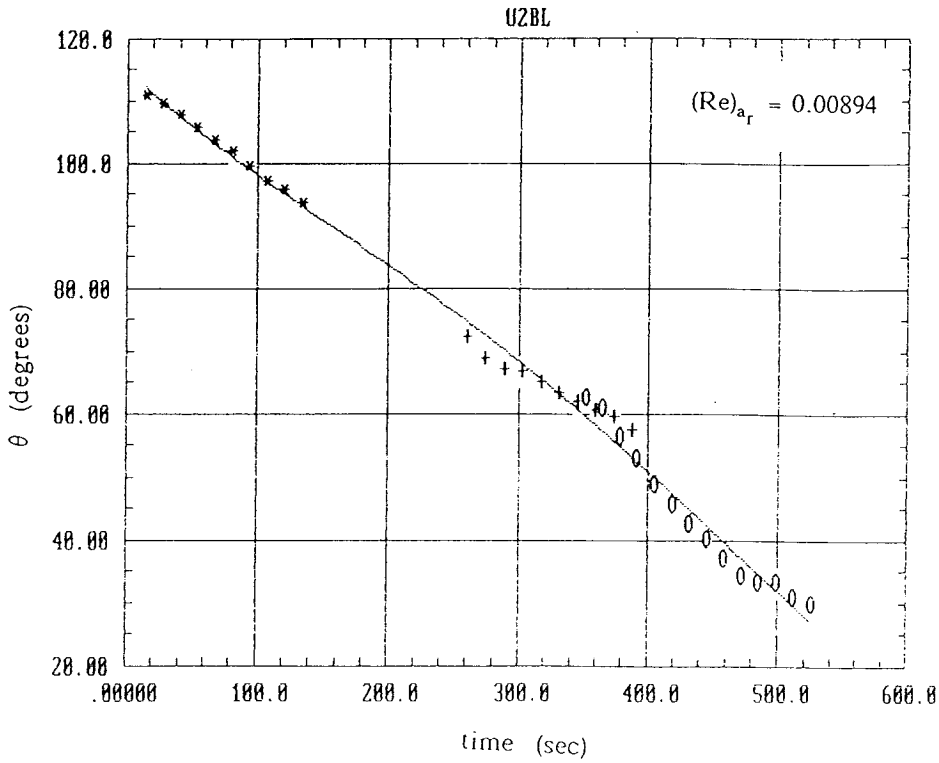

Figure 10(b). Time variation of θ for U2BL dendrite with ℓ/a = 3.80.

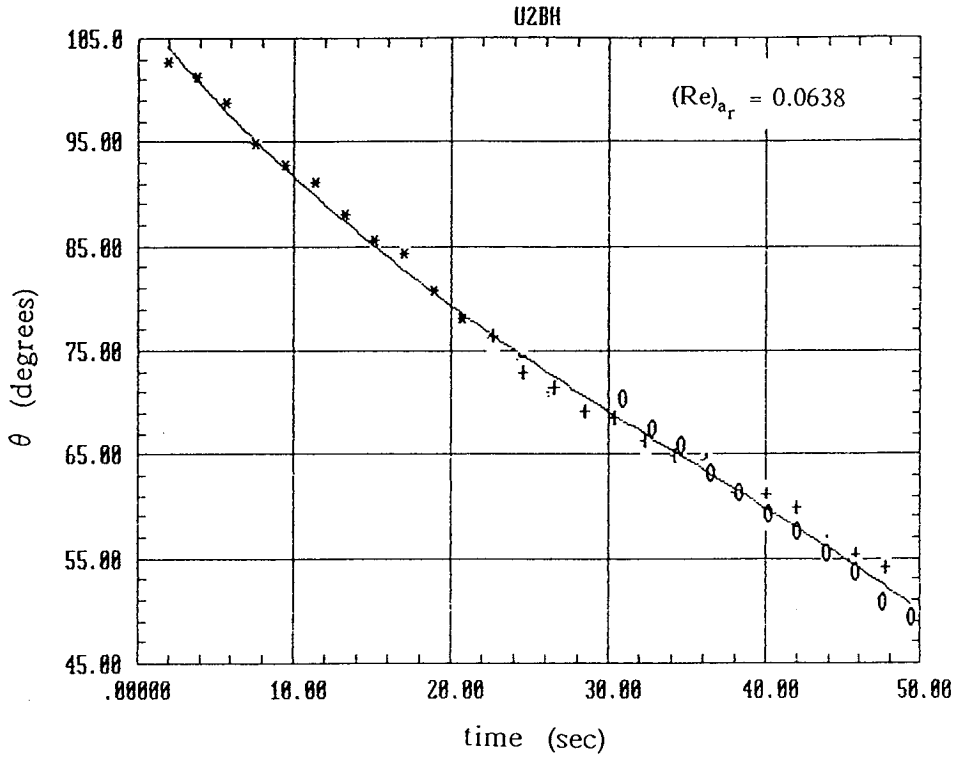

Figure 10(c). Time variation of θ for U2BH dendrite with ℓ/a = 3.80.

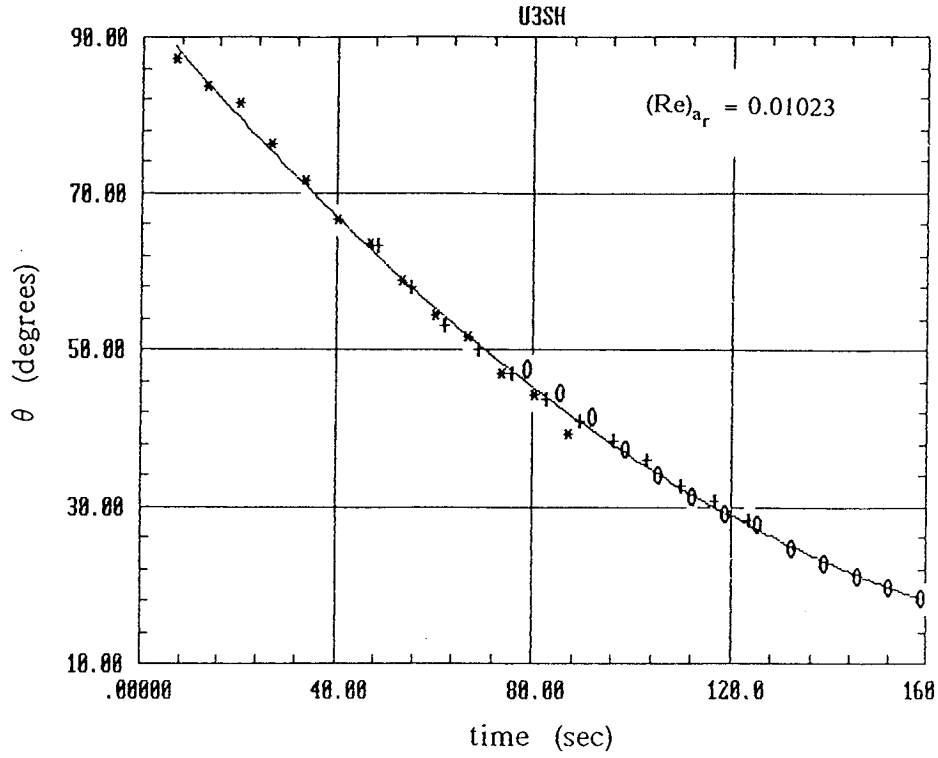

Figure 11(a). Time variation of θ for U3SH dendrite with ℓ/a = 4.40.

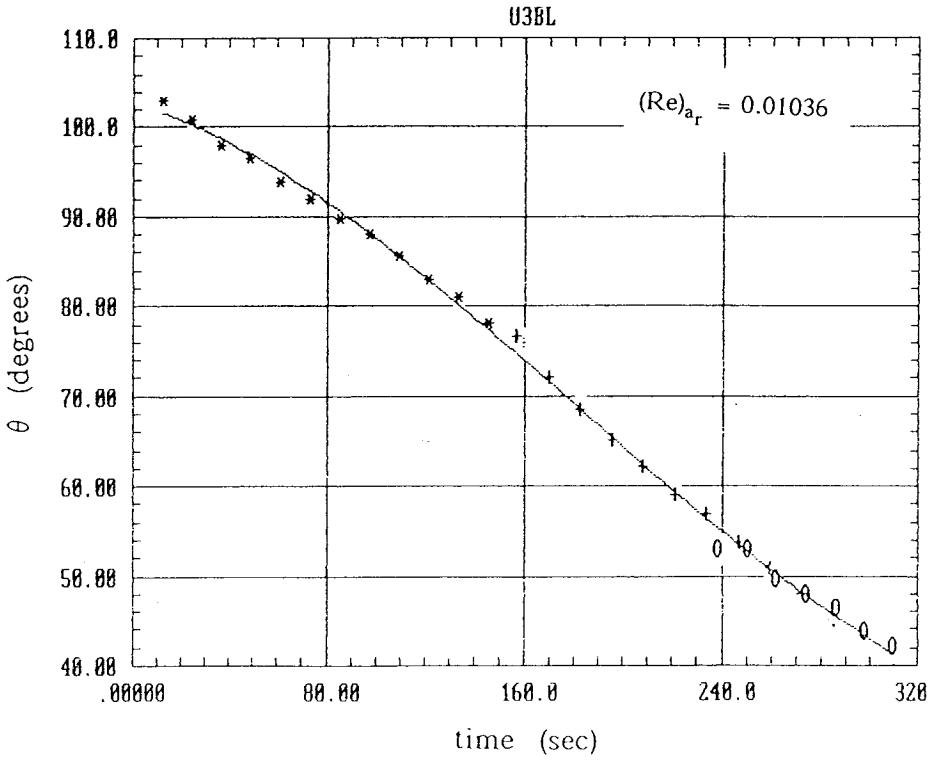

Figure 11(b). Time variation of θ for U3BL dendrite with ℓ/a = 4.40.

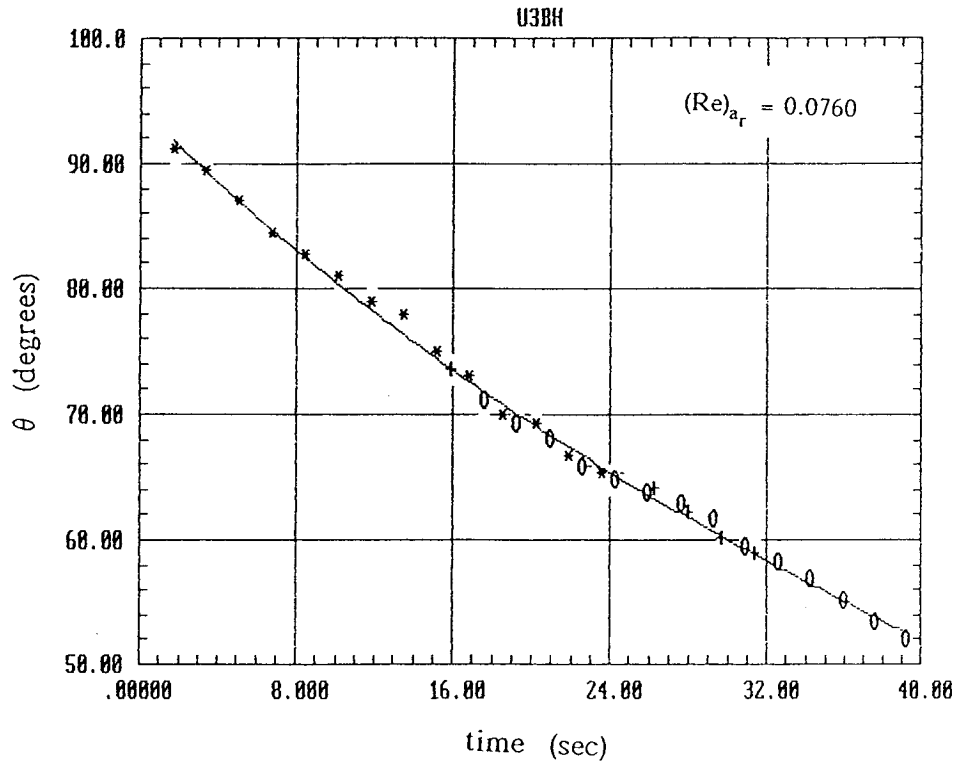

Figure 11(c). Time variation of θ for U3BH dendrite with ℓ/a = 4.40.

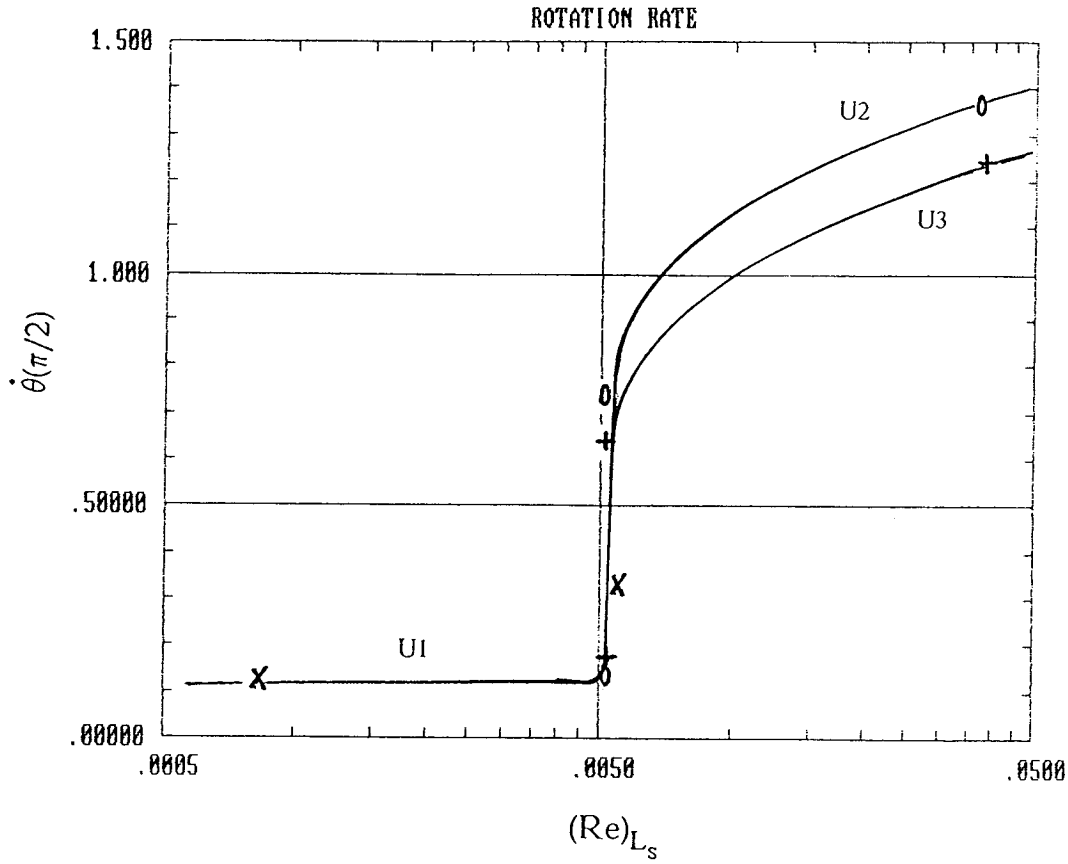

Figure 12. Rotation rate at $\theta = \pi/2$ for dendrites U1, U2, U3.